HHS Public Access

Author manuscript

Cell Rep. Author manuscript; available in PMC 2018 November 09.

Published in final edited form as:

Cell Rep. 2018 September 18; 24(12): 3312–3323.e5. doi:10.1016/j.celrep.2018.08.061.

A Tyrosine Switch on NEDD4-2 E3 Ligase Transmits GPCR Inflammatory Signaling

Neil J. Grimsey[1], **Rachan Narala**[1], **Cara C. Rada**[1,2], **Sohum Mehta**[1], **Bryan S. Stephens**[2,3], **Irina Kufareva**[3], **John Lapek**[1], **David J. Gonzalez**[1], **Tracy M. Handel**[3], **Jin Zhang**[1], and **JoAnn Trejo**[1,4,*]

[1]Department of Pharmacology, School of Medicine, University of California, San Diego, La Jolla, CA 92093, USA

[2]Biomedical Sciences Graduate Program, University of California, San Diego, La Jolla, CA 92093, USA

[3]Skaggs School of Pharmacy and Pharmaceutical Sciences, University of California, San Diego, La Jolla, CA 92093, USA

[4]Lead Contact

SUMMARY

Ubiquitination is essential for protein degradation and signaling and pivotal to many physiological processes. Ubiquitination of a subset of G-protein-coupled receptors (GPCRs) by the E3 ligase NEDD4–2 is required for p38 activation, but how GPCRs activate NEDD4–2 to promote ubiquitinmediated signaling is not known. Here, we report that the GPCR protease-activated receptor-1 (PAR1) stimulates c-Src-mediated tyrosine phosphorylation and activation of NEDD4–2 to promote p38 signaling and endothelial barrier disruption. Using mass spectrometry, we identified a unique phosphorylated tyrosine (Y)-485 within the 2,3-linker peptide between WW domain 2 and 3 of NEDD4–2 in agonist-stimulated cells. Mutation of NEDD4–2 Y485 impaired E3 ligase activity and failed to rescue PAR1-stimulated p38 activation and endothelial barrier permeability. The purinergic $P2Y_1$ receptor also required c-Src and NEDD4–2 tyrosine

*Correspondence: joanntrejo@ucsd.edu.

AUTHOR CONTRIBUTIONS

Conceptualization, N.J.G. and J.T.; Methodology, N.J.G., I.K., and J.T.; Investigation, N.J.G., R.N., C.C.R., S.M., J.L., B.S.S., and I.K.; Data Curation, N.J.G., J.L., and D.J.G.; Writing – Original Draft, N.J.G.; Writing – Review & Editing, N.J.G. and J.T.; Supervision, N.J.G. and J.T.; Funding Acquisition, N.J.G., T.M.H., I.K., J.L., C.C.R., and J.T.; Resources, D.J.G., J.Z., T.M.H., and J.T.

DATA AND SOFTWARE AVAILABILITY

Dataset and corresponding annotated spectra deposited in proteomeXchange; MassIVE: MSV000081998, ProteomeX Change:PXD008810

DECLARATION OF INTERESTS

There are no competing financial or other interests related to the work presented within this manuscript. Current affiliations as are stated except for the following: N.J.G. is an employee of the University of California, San Diego and the University of Georgia, Athens. J.L. is an employee of Pfizer.

SUPPLEMENTAL INFORMATION

Supplemental Information includes six figures and one table and can be found with this article online at https://doi.org/10.1016/j.celrep.2018.08.061.

phosphorylation for p38 activation. These studies reveal a novel role for c-Src in GPCR-induced NEDD4–2 activation, which is critical for driving ubiquitin-mediated p38 inflammatory signaling.

In Brief

Grimsey et al. report that GPCRs stimulate activation of NEDD4–2 E3 ubiquitin ligase via c-Src to induce endothelial p38 inflammatory signaling. c-Src phosphorylates NEDD4–2 at tyrosine-485, releasing the autoinhibitory linker peptide that is critical for enhancing E3 ligase activity, and provides mechanistic insight of how GPCRs activate E3 ubiquitin ligases.

Graphical Abstract

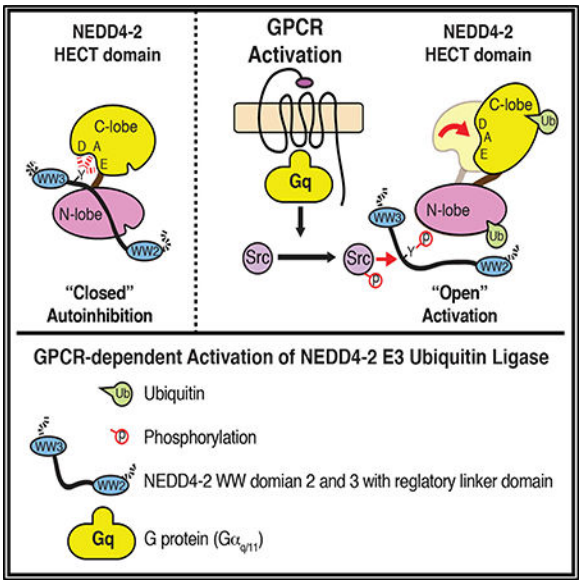

INTRODUCTION

G-protein-coupled receptors (GPCRs) are a ubiquitously expressed family of signaling receptors that have critical functions in numerous physiological processes. Dysfunction of GPCR signaling has been implicated in multiple diseases making this receptor class the largest target for approved drugs (Sriram and Insel, 2018). Despite recent advances in defining GPCR structure and pharmacology, many fundamental processes that control GPCR biology remain poorly understood. Extensive studies examining the role of phosphorylation in controlling GPCR signaling (Tobin, 2008) indicate that post-translational modifications are critical for governing receptor function. However, in contrast to phosphorylation, there is limited understanding of how ubiquitination of GPCRs is regulated.

The covalent attachment of ubiquitin to target substrates is known to regulate various aspects of protein function including stability, localization, and activity. Although ubiquitin can engender diverse functions, ubiquitination of mammalian GPCRs has been largely ascribed to degradative trafficking (Dores and Trejo, 2014). However, our recent study showed that GPCR ubiquitination can also drive inflammatory signaling through the recruitment of

transforming growth factor-β-activated kinase-1 binding protein-2 (TAB2) and TAB1, which triggers p38 auto-phosphorylation and activation (Grimsey et al., 2015). However, the mechanisms by which GPCRs activate E3 ubiquitin ligases to promote ubiquitin-mediated inflammatory signaling is not known.

Ubiquitin is covalently attached to substrate proteins by the sequential actions of E1, E2, and E3 ubiquitin enzymes. The family of NEDD4 (neural precursor cell expressed, developmentally downregulated-4) HECT (homologous to E6AP carboxyl terminus) domain-containing E3 ligases, where the E3 ubiquitin ligase confers substrate specificity, control diverse cellular functions and have been linked to the regulation of GPCR trafficking (Buetow and Huang, 2016; Jean-Charles et al., 2016; Scheffner and Kumar, 2014). However, while numerous studies have implicated NEDD4 E3 ligases in regulating GPCR function, it is not known how NEDD4 E3 ligases are released from auto-inhibition to increase HECT ubiquitin ligase activity following GPCR stimulation.

NEDD4 E3 ligases share similar domain architectures including an N-terminal localized C2-domain, two to four WW domains and a catalytic C-terminal HECT domain (Buetow and Huang, 2016). The activity of NEDD4 E3 ligases can be regulated through release of an auto-inhibited state, which occurs through allosteric mechanisms mediated by interactions with the C2 and WW domains (Bruce et al., 2008; Rotin and Kumar, 2009). Additionally, growth-factor-induced tyrosine phosphorylation of the C2 and HECT domain was shown to promote NEDD4–1 activation (Persaud et al., 2014), whereas serine phosphorylation of NEDD4 by various kinases inhibit activity (Rotin and Kumar, 2009). Two recent studies using biochemical, structural, and cellular analyses of overexpressed NEDD4 proteins unexpectedly discovered that peptide linkers tethering WW domains are critical regulators of E3 ligase catalytic activity. Specifically,Chen et al. showed that peptide linkers can lock the HECT domain in an inactive auto-inhibited state and propose that release of auto-inhibition is mediated by tyrosine phosphorylation of a peptide linker of WWP1, WWP2, NEDD4–1, and ITCH (Chen et al., 2017). In addition, the ITCH WW domain and following linker region allosterically locks the E3 ligase in an inactive state that can be relieved by binding of Ndfip1 or JNK1 phosphorylation (Zhu et al., 2017). However, the mechanisms and pathways that promote NEDD4–2 activation were not identified in either study. Here, we report that GPCRs stimulate NEDD4–2 ubiquitin ligase activity through c-Src-dependent tyrosine phosphorylation of the 2,3-linker peptide to promote p38 inflammatory signaling. These studies reveal an unexpected role for c-Src as a key regulator of NEDD4–2 activity, which is critical for driving ubiquitin-mediated inflammatory p38 signaling induced by the GPCRs, protease-activated receptor-1 (PAR1), and the purinergic $P2Y_1$ receptor, in endothelial cells.

RESULTS

Activated PAR1 Co-associates with and Activates NEDD4–2

We have shown that the GPCRs, PAR1, and $P2Y_1$ are ubiquitinated by the E3 ligase NEDD4–2 following agonist stimulation in endothelial cells (Grimsey et al., 2015). However, it is not known how GPCRs control NEDD4–2 activity. To determine whether NEDD4–2 is recruited to GPCRs, human endothelial cells were stimulated with thrombin and endogenous PAR1 immunoprecipitated (IP'ed). Thrombin-induced a rapid ~2-fold

increase in endogenous NEDD4–2 co-association with activated PAR1 (Figure 1A, lanes 2–4). Immunofluorescence confocal microscopy was then used to examine the subcellular localization of endogenous PAR1 and NEDD4–2. In control cells, PAR1 localized mainly to the cell surface displaying minimal ~15% colocalization with endogenous NEDD4–2 (Figures 1B and 1C). However, after thrombin stimulation, PAR1 internalized to endocytic vesicles and showed a significant ~30% co-localization with endogenous NEDD4–2 (Figures 1B and 1C). To verify colocalization of endogenous PAR1 and NEDD4–2, Pearson's correlation coefficients were calculated for control ($r = 0.025 \pm$ SD) and thrombin-treated conditions ($r = 0.165 \pm$ SD) (Figure 1D). These findings are consistent with rapid agonist-induced PAR1 internalization to early endocytic vesicles (Grimsey et al., 2015) and co-localization with NEDD4–2.

Thrombin Induces NEDD4–2 Activity Independent of Ca^{2+} Mobilization

Next, we examined whether thrombin activation of PAR1 regulates NEDD4–2 ubiquitin ligase activity. Thrombin-induced a significant 2.5-fold increase in NEDD4–2 auto-ubiquitination (Figure 1E, lanes 2 and 3). Thus, activated PAR1 recruitment of NEDD4–2 coincides with increased NEDD4–2 ubiquitination, an indication that the catalytic activity of NEDD4–2 is increased.

Previous reports showed that auto-inhibition of NEDD4–2 is mediated by the N-terminal C2 domain interaction with the HECT catalytic domain (Bruce et al., 2008), which can be released by intracellular Ca^{2+} to enhance NEDD4–2 activity (Wang et al., 2010). Despite thrombin's capacity to induce rapid mobilization of intracellular Ca^{2+} (Figure S1A), chelation of intracellular Ca^{2+} with BAPTA-AM failed to block thrombin-stimulated NEDD4–2 ubiquitination (Figure S1B). These findings indicate that thrombin-induced increase in NEDD4–2 ligase activity is Ca^{2+} independent, raising the intriguing idea that NEDD4–2 activity may be regulated by GPCRs through a different mechanism.

GPCR-Stimulated NEDD4–2 Activity and Ubiquitin-Mediated Signaling Is Initiated at the Plasma Membrane

To determine whether PAR1 internalization is required for NEDD4–2 activation and ubiquitin-mediated p38 signaling, we used a dynamin inhibitor Dyngo 4a (McCluskey et al., 2013). Thrombin-induced PAR1 internalization was blocked in Dyngo4a-pretreated cells (Figures 1F, S2A, and 1H). Dyngo 4a also caused a significant increase in NEDD4–2 co-localization with activated PAR1 at the plasma membrane (Figure 1F), confirmed by Pearson's correlation coefficients ($r = 0.328 \pm$ SD) compared to control cells ($r = 0.177 \pm$ SD) (Figure 1G). Agonist-induced PAR1 ubiquitination was also significantly enhanced in Dyngo4a-treated cells (Figure 1I), consistent with retention of the active PAR1-NEDD4–2 complex at the plasma membrane. We next assessed whether Dyngo 4a effected agonist-induced p38 activation. Thrombin increased p38 phosphorylation that peaked at 5 min and then decreased at 7.5 min in control cells (Figure 1J, lanes 1–5). In contrast, thrombin activation of p38 signaling was sustained up to 10 min in Dyngo-4a-treated cells (Figure 1J, lanes 6–10). A sustained increase in thrombin-induced p38 activation was also observed in cells in which PAR1 internalization was blocked by small interfering RNA (siRNA)-mediated depletion of AP-2 and epsin-1, clathrin adaptors required for activated PAR1

internalization (Chen et al., 2011) (Figures S2B–S2D). Thus, thrombin initiates recruitment of NEDD4–2 to PAR1 at the plasma membrane, and PAR1 internalization is not obligatory for NEDD4–2 ubiquitin-driven p38 signaling.

Thrombin-Induced Rapid c-Src Activation via G_q and $G_{12/13}$ Proteins

A recent study showed that growth-factor-dependent activation of c-Src increases ubiquitin ligase activity of NEDD4–1, a closely related homolog of NEDD4–2 (Persaud et al., 2014). While GPCRs are known to signal through c-Src, it is not known whether thrombin-activated PAR1 stimulates c-Src activity to promote NEDD4–2 activation and was examined by assessing c-Src tyrosine (Y)-419 auto-phosphorylation (Smart et al., 1981). Thrombin significantly increased c-Src Y-419 phosphorylation (Figure 2A, lanes 1–4), which was virtually abolished in cells pretreated with PP2, a Src family kinase inhibitor (Figure 2A,lanes 5–8). To examine the spatial and temporal changes in c-Src activity following thrombin stimulation, plasma-membraneassociated Kras-Src (pm-Kras-Src) or cytosolic-Src (cyto-Src) fluorescence resonance energy transfer (FRET) biosensors (Lu et al., 2008) were expressed in endothelial cells. Thrombin caused rapid c-Src activation resulting in changes in FRET ratios for both pm-Kras-Src and cyto-Src biosensors in multiple cells (Figures 2B and 2C). In all cases, thrombin-induced changes in FRET ratios were blocked after addition of PP2 (Figures 2B and 2C), indicating that the change in FRET requires c-Src activity. However, the rate of thrombin-induced activation of the cyto-Src biosensor was significantly delayed compared to the pm-Kras-Src biosensor (Figure 2D). Collectively, these data suggest that thrombin induces rapid c-Src activity at the plasma membrane that persists in the cytosol.

The mechanisms by which GPCRs activate c-Src are diverse and include direct binding to the receptor, Gα and βγ subunits, and β-arrestins (Luttrell and Luttrell, 2004). Given the rapid kinetics of c-Src activation induced by thrombin and the coupling of PAR1 to multiple heterotrimeric G protein subtypes, we examined the function of $G\alpha_q$ and $G\alpha_{12/13}$ subunits using siRNAs (Soto et al., 2015). Thrombin significantly increased c-Src phosphorylation at 2.5 min in non-specific siRN-transfected cells (Figure 2E, lanes 1 and 5) that was markedly reduced in $G\alpha_q$ and $G\alpha_{12/13}$-depleted cells (Figure 2E, lanes 5–8), suggesting a function of G proteins in thrombin-activated PAR1-stimulated c-Src activity. Moreover, chelation of intracellular Ca^{2+} failed to effect thrombin-induced c-Src phosphorylation, indicating that Ca^{2+} is unlikely to mediate c-Src activation or NEDD4–2 activity (Figures S1C and S1B).

Thrombin Stimulates c-Src-NEDD4–2 Association and c-Src-Dependent NEDD4–2 Activity

To determine c-Src function in thrombin-stimulated NEDD4–2 ligase activity, NEDD4–2-c-Src association and c-Src regulation of NEDD4–2 activity was examined. Thrombin induced a 3-fold increase in endogenous c-Src association with NEDD4–2 that peaked as early as 1 min and remained associated at 5 min (Figure 3A, lanes 2–4). To assess the role of c-Src in thrombininduced NEDD4–2 ligase activity, cells were treated with or without the PP2 inhibitor. In control cells, thrombin caused a marked ~2-fold increase in NEDD4–2 ubiquitination (Figure 3B, lanes 1 and 2), which was virtually abolished in cells incubated with PP2 (Figure 3B, lanes 3 and 4). These results suggest that thrombin promotes c-Src-NEDD4–2 co-association and requires c-Src function for stimulation of NEDD4–2 activity.

To further explore how c-Src regulates NEDD4–2 function, we examined NEDD4–2-PAR1 co-association and ubiquitination of PAR1 (Grimsey et al., 2015). Thrombin promoted PAR1-NEDD4–2 co-association (Figure 3C, lanes 1 and 2), whichwas effectively blocked in PP2-treated cells (Figure 3C, lanes 3 and 4). Thus, c-Src regulates NEDD4–2 activity and association with PAR1 following thrombin stimulation. Since NEDD4–2 is the key mediator of PAR1 ubiquitination, we examined whether ubiquitination of PAR1 is also regulated by c-Src. Thrombin induced a marked ~2.5-fold increase in PAR1 ubiquitination (Figures 3D and 3E, lanes 1 and 2), which was significantly reduced in PP2-treated cells and c-Src-depleted cells (Figures 3D and 3E, lanes 3 and 4). Depletion of c-Src by siRNA did not affect PAR1 expression (Figures 3E and S3A). These findings indicate that c-Src is a key regulator of thrombin-induced NEDD4–2 activity.

c-Src Is Required for PAR1-Stimulated p38 Signaling and TAB1 Stabilization

Ubiquitination of PAR1 drives non-canonical TAB1-mediated p38 activation in endothelial cells (Grimsey et al., 2015). Since our results indicate that c-Src regulates NEDD4–2 activity and mediates PAR1 ubiquitination, we examined whether c-Src activity is required for thrombin-induced p38 activation. Thrombin caused a marked increase in p38 phosphorylation in control cells (Figure 4A, lanes 1–4), which was significantly inhibited by PP2 (Figure 4A, lanes 5–8) but not by the analog PP3 (Figure 4A, lanes 9–12), a negative control for PP2 (Traxler et al., 1997). In contrast to p38, thrombin-induced ERK1/2 activation (Figure 4A, lanes 1–4) remained intact in PP2 and PP3-treated cells (Figure 4A, lanes 5–12), indicating that c-Src specifically regulates thrombin-stimulated p38 activation. Similar results were observed in thrombin-stimulated cells depleted of c-Src using siRNAs (Figure 4B). Moreover, induction of p38 phosphorylation by the cytokine tumor necrosis factor-α (TNF-α) was not affected by PP2 treatment (Figure S3B) nor by siRNA-mediated depletion of c-Src (Figure S3C). These findings indicate that c-Src specifically regulates GPCR-induced p38 activation and not ERK1/2 signaling nor TNF-α-induced p38 activation.

To determine whether the c-Src-NEDD4–2-p38 inflammatory signaling pathway is relevant to other GPCRs, we examined whether c-Src is required for ADP-induced p38 activation in endothelial cells. We previously showed that ADP activation of the GPCR $P2Y_1$ also promotes NEDD4–2- and ubiquitin-mediated p38 activation (Grimsey et al., 2015). Pretreatment of endothelial cells with PP2 or depletion of c-Src by siRNA blocked ADP-induced p38 activation (Figures S4A and S4B). In addition, c-Src activation induced by ADP is critically dependent on $G\alpha_q$ signaling (Figure S4C). These data indicate that c-Src is also a critical mediator of ADP-stimulated ubiquitin-mediated p38 activation in endothelial cells.

TAB1 expression is dynamically regulated by p38 signaling following thrombin activation of PAR1 in endothelial cells (Grimsey et al., 2015). However, it is not known whether c-Src also functions in the p38 pathway to regulate TAB1 expression. Thrombin caused a rapid and significant 2-fold increase in TAB1 expression within 2.5 min (Figure 4C, lanes 1–4), which was significantly inhibited by PP2 (Figure 4C, lanes 5–8). Depletion of c-Src by siRNA also blocked thrombin-induced increase in TAB1 expression (Figure 4D, lanes 5–8), compared to non-specific transfected cells (Figure 4D, lanes 1–4). Together, these results

indicate that c-Src function is pivotal for regulating NEDD4–2 ligase activity, ubiquitination of PAR1, and induction of non-canonical TAB1-mediated p38 activation.

NEDD4–2 Tyrosine-485 Phosphorylation Is Induced by Thrombin

To determine the mechanism by which c-Src regulates NEDD4–2 ligase activity, we examined whether thrombin induced NEDD4–2 tyrosine phosphorylation through a c-Src-dependent mechanism. Tyrosine phosphorylated proteins were IP'ed from thrombin-stimulated endothelial cells, and the presence of endogenous NEDD4–2 was detected by immunoblotting. Thrombin caused a rapid 2.5-fold increase in NEDD4–2 tyrosine phosphorylation (Figure 5A, lanes 1–3), which was blocked by PP2 (Figure 5A, lanes 4–6), suggesting that c-Src mediates NEDD4–2 tyrosine phosphorylation following thrombin stimulation. To identify the specific tyrosine phosphorylated sites induced by thrombin, we used global phospho-proteomics-based mass spectrometry. Endothelial cells treated with thrombin were lysed, processed, and enriched for phospho-peptides followed by labeling with tandem mass tag reagents, pooled, and subjected to mass spectrometry. A total of >24,000 non-redundant phospho-peptides were identified and quantified, including two NEDD4–2 peptides containing phosphorylated tyrosine-485 (Y485) residue (Table S1, MassIVE: MSV000081998, ProteomeX Change: PXD008810). Importantly, a significant ~2-fold increase in NEDD4–2 Y485 phosphorylation was detected in both phospho-peptides after thrombin treatment (Figure 5B). Intriguingly, Y485 resides within the linker peptide between WW domains 2 and 3 of NEDD4–2 (Figure 5B), raising the possibility that GPCR-mediated NEDD4–2 ligase activity is regulated by tyrosine phosphorylation of the 2,3-linker peptide.

Next, we determined whether phosphorylation of Y485 regulates NEDD4–2 ligase activity, using endothelial cells stably transduced with doxycycline inducible pSLIK lentiviral constructs encoding siRNA-resistant FLAG-tagged NEDD4–2 wildtype (WT) or Y485 to phenylalanine (F) mutant. A pSLIK construct encoding GFP was used as a control. Cells were depleted of endogenous NEDD4–2 by siRNA followed by doxycycline induction of siRNA resistance NEDD4–2 wild-type and Y485F mutant (Figure 5C, lanes 3–6) or GFP control (Figure 5C, lanes 1 and 2). Thrombin caused a significant increase in NEDD4–2 wild-type ubiquitination (Figure 5C, lanes 3 and 4), whereas no change in NEDD4–2 Y485F mutant ubiquitination was detected over control (Figure 5C, lanes 5 and 6). Neither NEDD4–2 nor changes in ubiquitination were detected in cells transduced with GFP (Figure 5C, lanes 1 and 2). These data suggest that activated GPCRs stimulate c-Src-mediated NEDD4–2 activity via tyrosine-485 phosphorylation.

NEDD4–2 Y485 Phosphorylation Is Required for Thrombin-Induced p38 Activation and Inflammatory Responses

To assess the function of NEDD4–2 Y485 phosphorylation in thrombin-induced inflammatory responses, we performed siRNA knockdown rescue experiments using NEDD4–2 wildtype and Y485F mutant. In cells transfected with non-specific siRNA-expressing GFP control, thrombin induced a robust increase in p38 phosphorylation (Figure 6A, lanes 1 and 2), which was markedly reduced in NEDD4–2 siRNA-transfected cells (Figure 6A, lanes 3 and 4). Expression of siRNA-resistant NEDD4–2 wild-type restored

thrombin-induced p38 phosphorylation to levels comparable to that observed in GFP controls cells (Figure 6A, lanes 5 and 6 versus 1 and 2). In contrast to NEDD4–2 wild-type, expression of the NEDD4–2 Y485F mutant failed to rescue thrombin-stimulated p38 phosphorylation (Figure 6A, lanes 5 and 6 versus 7 and 8), suggesting that tyrosine phosphorylation of the 2,3-linker peptide region of NEDD4–2 at Y485 is necessary for thrombin-stimulated p38 activation. We next assessed whether NEDD4–2 Y485 phosphorylation is necessary for ADP-induced p38 activation using a similar approach. In cells expressing NEDD4–2 wild-type, ADP-induced a significant increase in p38 phosphorylation (Figure S5, lanes 1 and 2), whereas in cells expressing the NEDD4–2 Y485F mutant ADP failed to induce p38 phosphorylation (Figure S5, lanes 3 and 4).

To assess the function of NEDD4–2 Y485 phosphorylation in GPCR-stimulated p38-mediated inflammatory responses, we examined thrombin-stimulated endothelial barrier permeability. Endothelial cells transfected with non-specific siRNA and expressing GFP, NEDD4–2 wild-type, or Y485F mutant exhibited a progressive increase in endothelial barrier permeability over control at various times following thrombin stimulation (Figure 6B). In cells depleted of NEDD4–2 by siRNA and expressing GFP, the capacity of thrombin to induce permeability was significantly reduced (Figures 6C and 6D). However, expression of wild-type NEDD4–2 restored thrombin-induced endothelial barrier permeability to a level comparable to that observed in nonspecific siRNA-transfected cells (Figures 6C and 6D). In contrast, expression of NEDD4–2 Y485F mutant failed to rescue thrombin-stimulated barrier permeability in cells deficient in endogenous NEDD4–2 (Figures 6C and 6D). Collectively, these data indicate that NEDD4–2 Y485 phosphorylation is necessary for thrombinand ADP-induced p38 activation and thrombin-mediated endothelial barrier disruption, revealing a critical role for tyrosine phosphorylation of NEDD4–2 in the regulation of GPCR-mediated endothelial inflammatory responses.

Model of NEDD4–2 Activation Induced by Tyrosine Phosphorylation of 2,3-Linker Peptide Stimulated by GPCRs

E3 ligase HECT domains comprise a large N-lobe that interacts with the E2 enzyme, a hinge region and C-lobe that mediates ubiquitin (Ub) transfer (Buetow and Huang, 2016) and exists either in a “closed” auto-inhibited or an “open” catalytically active state (Figure 7A). In recent studies, crystal structures of several HECT domains were solved to define the molecular basis of NEDD4 auto-inhibition. The structure of ITCH without the C2 domain revealed that the WW2 and 2, 3-linker is packed against the C-lobe of the HECT domain, locking ITCH into a closed autoinhibited confirmation (PDB 5×mc) (Zhu et al., 2017). Chen et al. showed a similar conformation for WWP2, where the WW2 and 2,3 linker peptide is fused directly to the HECT domain (PDB 5tj7 and 5tj8) (Chen et al., 2017). In WWP2 and ITCH, the C-terminal region of the 2,3-linker peptide, 15–20 residues preceding the WW3 domain, adopts an extended conformation that is packed against the C-lobe. A conserved tyrosine residue, Y392 in WWP2 and Y420 in ITCH, forms favorable hydrogen-bonding with a conserved acidic triad, D787, N788, and E789 in WWP2 and D820, N821, and E822 in ITCH (Chen et al., 2017; Zhu et al., 2017). While this is a relatively weak interaction, it forms a steric lock restricting the rotational shift of the C-lobe that is required for the “open,” Ub-, and E2-bound conformation (PDB 3jvz of the HECT domain of NEDD4–2,

PDB 3TUG for the HECT domain of ITCH) (Kamadurai et al., 2009; Zhu et al., 2017). Thus, it is conceivable that phosphorylation of the conserved tyrosine unlocks the C-lobe enabling its rotation to the “open” active conformation. While the 2,3-linker peptide region of NEDD4–2 bears low homology to the 2,3-linker peptides of WWP2 and ITCH, the critical Y485 in NEDD4–2 is located 14 residues preceding the WW3 domain, and thus Y485 in NEDD4–2 is positioned to assume structural and functional similarities to Y392 in WWP2 (Chen et al., 2017) and Y420 in ITCH (Yang et al., 2006; Zhu et al., 2017). To illustrate this hypothesis, we modeled the C-terminal region of the 2,3-linker of the WW domain 3 and 4 and the HECT domain of NEDD4–2 in both the “closed” and “open” conformations (Chen et al., 2017; Kamadurai et al., 2009; Zhu et al., 2017). The model suggests that Y485 in NEDD4–2 has access to a homologous acidic triad D891, A892, and E893 in the C-lobe of the HECT domain in the closed conformation (Figures 7A and 7B). Phosphorylation of Y485 in NEDD4–2 may disrupt the interaction with the acidic triad D891, A892, and E893 while simultaneously introducing electrostatic repulsion, and motion of the C-lobe (Figures 7B, 7C, and S6). Such structural changes of NEDD4–2 would result in an “open” active conformation observed crystallographically when NEDD4–2 is bound to ubiquitin and the E2 ligase UbcH5B (Kamadurai et al., 2009). These findings together with our biochemical and cellular studies strongly suggest that tyrosine phosphorylation of the 2,3-linker peptide of NEDD4–2 serves as a key regulatory element for GPCR stimulation of E3 ligase activity.

DISCUSSION

We previously showed that the HECT domain containing E3 ligase NEDD4–2 mediates GPCR ubiquitination to control receptor signaling rather than lysosomal degradation. Ubiquitination of PAR1 or the P2Y1 purinergic receptor was shown to initiate recruitment of a signaling complex comprised of TAB2, TAB1, and p38, which induces p38 auto-phosphorylation and activation (Grimsey et al., 2015). However, it is not known how NEDD4–2 is activated in response to GPCR stimulation. We now report that endothelial GPCRs initiate ubiquitin-driven p38 signaling through c-Src-mediated NEDD4–2 tyrosine phosphorylation and activation at the plasma membrane. Demonstrating that GPCRs functionally activate NEDD4–2 E3 ligase through a tyrosine phosphorylation switch that releases autoinhibition.

Over forty mammalian GPCRs have been reported to be ubiquitinated largely by the NEDD4 family E3 ligases (JeanCharles et al., 2016). However, the mechanism by which GPCRs induce activation of NEDD4 E3 ubiquitin ligases has not been established. Here, we demonstrate that PAR1 couples to $G\alpha_q$ or $G\alpha_{12/13}$ to induce rapid c-Src activation, switching on NEDD4–2 E3 ligase activity at the plasma membrane independent of Ca^{2+} mobilization. Activated P2Y1 receptor also couples to $G\alpha_q$ to induce NEDD4–2 activity through a similar mechanism. Interestingly, PAR1-stimulated ubiquitin-driven p38 signaling peaks when both PAR1 and TAB2 are present on early endocytic vesicles (Grimsey et al., 2015) suggesting that GPCR-TAB-p38 signaling complex assembles on endosomes. However, we found that PAR1 internalization is not required for NEDD4–2-dependent ubiquitin-mediated p38 signaling, indicating that activation of this pathway is likely initiated from the plasma membrane. Nonetheless, these data do not preclude the possibility that the

GPCR-TAB-p38 signaling complex remain associated after internalization and is competent to signal from endosomes

The transition from the inactive “closed” state to an “open” catalytically active state of HECT E3 ligase can be regulated by allosteric interactions with the C2 and WW domains and phosphorylation-dependent activation, although the mechanisms are not fully defined (Bruce et al., 2008; Escobedo et al., 2014; Gallagher et al., 2006; Persaud et al., 2014; Riling et al., 2015; Wiesner et al., 2007; Zhu et al., 2017). Additionally, the 2,3-linker of HECT family E3 ligases WWP2 and ITCH but not NEDD4–2 has been previously shown to regulate ligase activity through auto-inhibition (Chen et al., 2017). A distinct but conceptually related structural mechanism of HECT domain regulation occurs in HUWE1 E3 ligase auto-inhibitory dimers, at the dimer interface the pointer domain mimics the 2,3-linker domain of WWP2 and ITCH, locking the HECT domain into a closed conformation (Sander et al., 2017). These studies demonstrate that diverse mechanisms regulate E3 ligase activity including auto-inhibition by the 2,3-linker peptide.

Our studies suggest that NEDD4–2 Y485 enables the 2,3-linker to restrict the movement of the HECT domain C-lobe through interactions with the acidic triad (Figure 7). Interestingly, the 2,3-linker peptide of NEDD4–2 lacks structural conservation with the 2,3-linker peptide of WWP2 and is not predicted to assume an α-helical conformation. This would allow the 2,3-linker peptide of NEDD4–2 to serve as a better substrate for tyrosine phosphorylation since tyrosine kinases preferentially bind to extended conformations (Bose et al., 2006). While Chen et al. clearly show that tyrosine phosphorylation of the 2,3-linker domain is required for WWP2 activation, the kinases responsible for phosphorylation under physiological conditions were not identified (Chen et al., 2017). Our findings suggest that c-Src-dependent phosphorylation of the 2,3-linker peptide of NEDD4–2 disrupts the interaction with the acidic triad and enables movement of the C-lobe, facilitating a transition to the “open” active conformation (Figures 7B and S6). However, further biochemical and structural studies are needed to confirm the precise details by which the 2,3-linker peptide regulates activation of NEDD4–2 E3 ligase activity in response to GPCR stimulation.

Our studies highlight an important physiological function for the tyrosine switch in NEDD4–2 activation and GPCR-induced inflammatory signaling in endothelial cells. We demonstrate that PAR1 coupling to $G\alpha_q$ and $G\alpha_{12/13}$ stimulates c-Src-mediated NEDD4–2 activation and ubiquitin-driven p38 activation that promotes endothelial barrier disruption. We also found that this pathway is conserved for other GPCRs, specifically endothelial $P2Y_1$. While c-Src inhibitors have been shown to block GPCR-induced blood-brain barrier breakdown *in vivo*, the underlying mechanisms are not known (Liu et al., 2010). In fact, c-Src is known to directly regulate the endothelial barrier through modulation of the actin cytoskeleton and adherens junction components, including p120 and vascular endothelial (VE)-cadherin (Adam, 2015) and now NEDD4–2 activation. Thus, additional studies will be required to define the specific role of c-Src-mediated NEDD4–2 activation in GPCR-induced disruption of endothelial barrier *in vivo*.

In summary, these studies advance our understanding of how GPCRs stimulate E3 ligase activity by unlocking the auto-inhibited state in an important physiological context. These

findings further reveal a key role for c-Src in initiating GPCR-stimulated NEDD4–2 activity and ubiquitin-driven p38 signaling expanding the function of c-Src in inflammatory signaling.

STAR⋆METHODS

KEY RESOURCES TABLE

REAGENT or RESOURCE	SOURCE	IDENTIFIER
Antibodies		
Mouse IgG	Rockland Immunochemicals	Cat# 010–001-298; RRID:AB_832813
Mouse P4D1 (anti-ubiquitin)	Santa Cruz Biotechnology	Cat# sc-8017; RRID:AB_628423
Rabbit $G\alpha_{q/11}$ (clone C12)	Santa Cruz Biotechnology	Cat# sc-46972; RRID:AB_2279038
Rabbit $G\alpha_{12}$ (clone S20)	Santa Cruz Biotechnology	Cat# sc-409; RRID:AB_2263416
Rabbit $G\alpha_{13}$ (clone A20)	Santa Cruz Biotechnology	Cat# sc-410; RRID:AB_2279044
Mouse anti-GFP	Covance	Cat# MMS-118R-200; RRID: AB_10064222
Mouse anti-Thrombin receptor	Beckman Coulter	Cat# IM2085; RRID:AB_131681
Mouse M2 anti-Flag	Sigma-Aldrich	Cat# P2983; RRID:AB_439685
Mouse anti-beta actin	Sigma-Aldrich	Cat# A1978; RRID:AB_476692
Rabbit anti-NEDD4L	Cell signaling Technology	Cat# 4013S; RRID:AB_1904063
Rabbit anti-TAB1	Cell signaling Technology	Cat# 3226S; RRID:AB_2140247
Rabbit Anti-p38 MAPK, phospho (Thr180 / Tyr182) Monoclonal Antibody, Unconjugated, Clone D3F9	Cell signaling Technology	Cat# 4511L; RRID:AB_2139679
Rabbit monoclonal anti-p38 MAPK phospho -(Thr180/Tyr182) (D3F9)XP	Cell signaling Technology	Cat# 4511P; RRID:AB_2139685
Rabbit anti-p42/p44 MAPK	Cell signaling Technology	Cat# 9102; RRID:AB_330744
Mouse anti-phospho-p42/p44 MAPK	Cell signaling Technology	Cat# 9106; RRID:AB_331768
Rabbit anti-c-Src	Cell signaling Technology	Cat# 8077S; RRID:AB_10860048
Rabbit anti-phospho-c-Src (Y416)	Cell signaling Technology	Cat# 2101; RRID:AB_331697
Mouse anti-GAPDH	Genetex	Cat# GTX627408; RRID:AB_11174761
Mouse 4G10® platinum anti-phospho-tyrosine	Millipore	Cat# 05–1050X; RRID:AB_916370
HRP-conjugated goat-anti-rabbit	Bio-Rad Laboratories	Cat# 170–6515; RRID:AB_11125142
HRP-conjugated goat-anti-mouse	Bio-Rad Laboratories	Cat# 170–6516; RRID:AB_11125547
Alexa fluor 488 anti-mouse	Life Technologies	Cat# A-11029; RRID:AB_2534088
Alexa fluor 594 anti-rabbit	Life Technologies	Cat# A-11037; RRID:AB_2534095
Chemicals, Peptides, and Recombinant Proteins		
Human α-Thrombin (Factor IIa)	Enzyme Research Laboratories	Cat# HT 1002a; CAS: N/A
Adenosine Diphosphate	Acros Organics	Cat#AC164670010; CAS: 16178–48-6
TNF-α	EMD Millipore	Cat# 635343; CAS N/A
SB-203580	Sigma Aldrich	Cat# S8307; CAS:152121–47-6

REAGENT or RESOURCE	SOURCE	IDENTIFIER
PP2	Sigma Aldrich	Cat#529573; CAS: 172889–27-9
PP3	Sigma Aldrich	Cat# 529574; CAS: 5334–30-5
BAPTA-AM	Sigma Aldrich	Cat# A1076; CAS:126150–97-8
MG-132	Sigma Aldrich	Cat# 474790; CAS: 133407–82-6
PR-619	Tocris	Cat# 4482; CAS: 2645–32-1
Dyngo 4a	Abcam	Cat# ab120689; CAS: 1256493–34-1
Deposited Data		
Dataset and corresponding annotated spectra deposited in proteomeXchange using MassIVE	http://www.proteomexchange.org/	MassIVE: MSV000081998
Dataset and corresponding annotated spectra	http://www.proteomexchange.org/	ProteomeXChange: PXD008810
Experimental Models: Cell Lines		
EA.hy 926 endothelial cells	ATCC	Cat# CRL-2922, RRID: CVCL_3901
Primary Human Umbilical Vein Endothelial Cells (HUVECs), pooled donor in EGM™	Lonza	Cat# CC-2519
Oligonucleotides		
siRNA targeting sequence: Allstars negative control	QIAGEN	Cat # 1027281
c-Src specific siRNA oligonucleotide #7 5'-GCUUGUGGGU GAUGUUUGATT-3'	QIAGEN	Cat # SI02223928
siRNA targeting sequence: NEDD4–2 siRNA oligonucleotide #7 5'-GAAUAUCGCUGGAGACUCU-3'	QIAGEN	Custom siRNA, Grimsey et al., 2015
siRNA targeting sequence: Adaptor protein subunit μ2: 5'-GTGGATGCCTTTCGGGTCA-3'	QIAGEN	Custom siRNA, Chen et al., 2011
siRNA targeting sequence: EPSN1: 5'-GGAAGACGCCG GAGTCATT-3'	QIAGEN	Custom siRNA, Chen et al., 2011
siRNA targeting sequence: $G\alpha_{q/11}$: 5'-GAUGUU-CGUGG ACCUGAAC-3'	QIAGEN	Custom siRNA, Soto et al., 2015
siRNA targeting sequence: $G\alpha_{12}$: 5^0-GGAUCGGCCAGC UGAAUUATT-3'	QIAGEN	Custom siRNA, Soto et al., 2015
siRNA targeting sequence: $G\alpha_{13}$: 5'-CGACUGCUUACC AAAUUAATT-3'	QIAGEN	Custom siRNA, Soto et al., 2015
Recombinant DNA		
pEN_TmiRc3	Addgene	https://www.addgene.org/25748/
pSLIK-hygro	Addgene	https://www.addgene.org/25737/
pMDLg/pRRE	Addgene	https://www.addgene.org/12251/
pRSV-Rev	Addgene	https://www.addgene.org/12253/
pMD2.G/pVSV-G	Addgene	https://www.addgene.org/12259/
pSLIK-hygro-GFP	This paper	N/A

REAGENT or RESOURCE	SOURCE	IDENTIFIER
pSLIK-hygro-FLAG-NEDD4–2 wild-type siRNA #7 resistant	This paper	N/A
pSLIK-hygro-FLAG-NEDD4–2 Y485 siRNA #7 resistant	This paper	N/A
Software and Algorithms		
Metamorph	Molecular Devices	N/A
ImageJ	NIH	https://imagej.nih.gov/ij/
ProteomeDiscoverer 2.1.0.81 software package		https://software.broadinstitute.org/GENE-E/index.html
Metafluor 7.7	Molecular Devices	https://www.moleculardevices.com/products/cellular-imaging-systems/acc
Prism 7.0, Statistical analysis software	Graphpad	https://www.graphpad.com/scientificsoftware/prism/
Uniprot database of Human entries		https://www.uniprot.org/downloads
ICM-Pro, version 3.8–6	Molsoft LLC	http://www.molsoft.com

CONTACT FOR REAGENT AND RESOURCE SHARING

Further information and requests for resources and reagents should be directed to and will be fulfilled by the Lead Contact, JoAnn Trejo (joanntrejo@ucsd.edu).

EXPERIMENTAL MODEL AND SUBJECT DETAILS

Cell lines—Primary human umbilical vein endothelial cells (HUVECs, pooled vein donor samples) cultured in endothelial growth media plus (Lonza Ltd.) at 37°C at 5% $C0_2$. HUVEC–derived EA.hy926 cells were cultured using 10% FBS and Dulbecco's Modified Eagles Media at 37°C at 5% $C0_2$.

CDNA—Pm-Src-KRas and the cyto-Src biosensors were from the Dr. Peter Yingxiao Wang (UC San Diego). The pCI-FLAG-NEDD4–2 was from Dr. Wesley Sundquist (The University of Utah). The siRNA resistant NEDD4–2 was generated by QuikChange site-directed mutagenesis (Agilent Technologies) mutating nucleotides c846t, t849a, a852t, t856a and t858a, confirmed by dideoxy sequencing. Tyrosine Y-485 (Y485F) was mutated to phenylalanine (F) by site-directed mutagenesis. NEDD4–2 siRNA resistant wild-type and Y485F were cloned into a pSLIK lentiviral vector and EA.hy926 stable lines generated as described (Chen et al., 2014).

Cell transfections—EA.hy926 cells were seeded at 1.4×10^5 of 24-well plates and grown overnight. HUVECs were seeded at 1.2×10^5 per well of a 24-well plate coated with $10\mu g/cm^2$ rat tail collagen type I. Cells were transfected with siRNA using Oligofectamine (Life Technologies), for EA.hy926 and TransIT-X2 (Mirus) for HUVECs, per the manufacturer's instructions (see Key Resources Table for specific siRNA sequences). FRET biosensor expression plasmids were transfected into cells seeded on Matek imaging plates, using X-tremeGENE HP (Roche) per manufacturer's instructions.

METHOD DETAILS

Cell surface ELISA—The expression of endogenous PAR1 was measured by ELISA as previously described (Grimsey et al., 2015; Soto and Trejo, 2010). Cells were fixed with 4% paraformaldehyde, washed and incubated with anti-PAR1 antibody and followed by incubation with antimouse IgG conjugated to HRP. Surface PAR1 detected using HRP substrate one-step 2,2'-azinobis-3-ethylbenzthiazoline-6-sulfonic acid (ThermoFisher Scientific) 20 min at RT. Absorbance at 405 nm was measured using a Molecular Devices SpectraMax Plus microplate reader. Each experimental condition was in triplicate and averages were taken from three independent repeats.

Immunofluorescence confocal microscopy—Cells grown on coverslips and processed for immunofluorescence microscopy as described (Grimsey et al., 2015). Serum starved cells were pretreated (as indicated) with 15 μM Dyngo 4a for 30 min prior to 10 nM α-Th. Percent overlap and Pearson's correlation coefficients (*r*) were calculated using MetaMorph 7.7 software (Molecular Devices). Images were collected blind > 3 images per condition, data collected from three independent repeats.

FRET Live-cell imaging—Cells were transfected with cytosolic or KRas-targeted (Lu et al., 2008) Src biosensors. After 24 h, cells were incubated in Hank's Balanced Salt Solution (HBSS) with 20 mM HEPES pH7.4, 5 mM D-glucose and 0.23 mM sodium pyruvate for 1 h before addition of 10 μM α-Th and 10 mM PP2. Image acquisition and FRET measurements were as described (Mehta and Zhang, 2014). Cells were analyzed using MetaFluor 7.7 by defining a region of interest (ROI) that encompassed each complete endothelial cell. The cyan fluorescent protein (CFP)/ yellow fluorescent protein (YFP) emission ratios were normalized to the value immediately before thrombin addition and used to calculate the FRET signals. Greater than 3 images were collected blind per condition, presented data collected from the average of three independent repeats.

Immunoblotting—Cells were transfected and grown as described above and pretreated (as indicated) with 5 mM PP2, 5 μM PP3 or 15 μM Dyngo 4a for 30 min prior to stimulation with 10 nM α-Th or 10 μM ADP. Cells were lysed in 1X Laemmli sample buffer with 100 mM DTT, sonicated and resolved by SDS-PAGE. Immunoblots were quantified by densitometry using ImageJ software.

Immunoprecipitations—Cells were stimulated with agonists and processed as described (Grimsey et al., 2016) except with Triton lysis buffer containing 20 μM PR619. EA.hy926 cells were grown in 6 cm dishes, serum starved overnight and lysed in Triton lysis buffer containing 50 mM Tris-HCl pH 7.4, 100 mM NaCl, 1% Triton X-100, 10 mM NaF, 10 mM β-glycerophosphate, 10 mM NaPP, 2mM $NaVO_4$, 10 μg/ml leupeptin, aprotinin, trypsin protease inhibitor, pepstatin, 100 μg/ml benzamide, 20 mM N-ethylmaleimide and 20 μM PR619. Cell lysates were homogenized, cleared by centrifugation and protein concentrations determined by bicinchoninic acid assay (BCA). Equivalent amounts of lysates were used for immunoprecipitations using the anti-phospho-tyrosine antibody (4G10 Platinum, Millipore) samples were eluted with 2X Laemmli sample buffer containing 200 mM dithiothreitol, resolved by SDS-PAGE and developed by chemiluminescence. Aliquots of cell lysates were

also immunoblotted with specific antibodies as indicated. Co-IP of endogenous PAR1 and NEDD4–2 were performed as above except 1% Triton X-100 was replaced with 1% n-dodecyl-β-D-maltoside (DDM) lysis buffer. PAR1 ubiquitination assays were performed as previously described(Grimsey et al., 2015). Cell were serum starved overnight and lysed in RIPA buffer containing 50 mM Tris-HCl pH 8.0, 150 mM NaCl, 5 mM EDTA, 1% NP-40, 0.5% sodium deoxycholate, 0.1% SDS, 10 mM NaF, 10 mM β-glycerophosphate, 10 mM NaPP, 2 mM $NaVO_4$, 10 mg/ml leupeptin, aprotinin, trypsin protease inhibitor, pepstatin, 100 μg/ml benzamide, 20 mM N-ethylmaleimide and 20 μM PR619.

Calcium Assays—Cells were grown in 96-well black clear bottom plates (Becton Dickinson Labware), washed with PBS and loaded with Fluo-4NW (Life Sciences) and probenecid (2.5 mM) in HBSS followed by the addition of DMSO or BAPTA-AM (10 μM). Cells challenged with 10 nM α-Th at 37°C, fluorescence intensity (excitation 485 nm, emission 525 nm) monitored every 2 s immediately using a FLIPR plate reader (Molecular Devices). Ca^{2+} is presented as the ratio of sample fluorescence at any given time point (F) divided by background fluorescence (F0). For each independent repeat, all experimental conditions were in triplicate and assayed simultaneously on the same plate.

Endothelial barrier permeability—Endothelial barrier permeability was quantified by measuring the flux of Evans blue-bound BSA as previously described (Grimsey et al., 2015). EA.hy926 cells were seeded into 3.0 μM transwell permeability support chambers (Corning), and grown for 5 days. The cells were starved overnight and treated as indicated. Evans blue conjugated to BSA was added to the upper chamber after 10 min of agonist stimulation at 37°C. Samples were removed from the lower chamber at the indicated time points and the amount of Evans blue diffusion was quantified by measuring the absorbance at 605 nm using a microplate reader (SpectraMax Plus, Molecular Devices).

Mass Spectrometry Based Proteomics—EA.hy926 cells were grown in 150 cm2 dishes and starved overnight, stimulated with 10 nM α-Th, washed with PBS, lysed in 3% SDS, 75 mM NaCl, 1 mM NaF, 1 mM beta-glycerophosphate, 1 mM sodium orthovanadate, 10 mM sodium pyrophosphate, 1 mM PMSF and 1X Roche Complete mini EDTA free protease inhibitors in 50 mM HEPES, pH8.5. Lysates were homogenized, sonicated, centrifuged, and the supernatants processed for LCMS2/MS3 analysis, data processing and analysis as previously described (Lapek et al., 2017).

Lyophilized peptides were re-suspended and labeled with tandem mass tag (TMT), pooled into multiplex experiments, and fractionated by HPLC. Identification and quantification of peptides by LC-MS2/MS3. All LC-MS2/MS3 experiments were performed on an Orbitrap Fusion mass spectrometer with an in-line Easy-nLC 1000 with chilled autosampler. Data processing and analysis was performed using ProteomeDiscoverer 2.1.0.81. SequestHT was utilized to assign identities to MS2 spectra searching against the Uniprot database of Human entries (downloaded Feb. 27, 2016 with 69,961 total entries). Including a 50 ppm MS1 mass tolerance and 0.6 Da fragment ion tolerance. Data were filtered to a peptide and protein false discovery rate of less than 1%. TMT reporter ion intensities were extracted from MS3 spectra for quantitative analysis. Spectra used only if greater than 10 × average signal to noise per label and isolation interference of less than 25%. Data were normalized as

previously described (Lapek et al., 2017). The dataset and annotated spectra are deposited in ProteomeXchange through MassIVE (ProteomeXChange: PXD008810, MassIVE: MSV000081998).

Molecular Modeling of NEDD4–2 (aa 480–970)—A continuous fragment of NEDD4–2 containing a part of the WW2-WW3 linker, WW3 and WW4 domains, and the HECT domain was modeled using ICM-Pro software, version 3.8–6 (MolSoft LLC, San Diego, CA) (Abagyan and Totrov, 1994). The open conformation of the HECT domain was taken from PDB 3jvz (Kamadurai et al., 2009), and the closed conformation modeled by homology using the structure of the corresponding domain of WWP2 (PDB 5tj7)(Chen et al., 2017). A single polypeptide chain containing the C-terminal part of the WW2-WW3 linker (residues 480–497), the WW3 domain (residues 498–531), the entire WW3-WW4 linker (residues 532–546), the WW4 domain (residues 547–587), and the WW4-HECT linker (residues 588–600) was built by homology to the WW3 and WW4 domains of ITCH (PDB 5cq2)(Liu et al., 2016), with the linkers built *ab initio*. The backbone atoms of residues 480–488 were tethered with harmonic restraints to residues 387–395 of the WWP2 structure, assuming correspondence of NEDD4–2 Y485 to WWP2 Y392 and, the backbone atoms of residues 597–600 were tethered to the corresponding atoms in the NEDD4L HECT domain structure (for the open conformation) or model (for the closed conformation). The NEDD4–2 HECT domain residues not involved in restraints, as well as the bound Ub and E2 molecules for the open conformation, were represented as potentials calculated on a 0.5 A˚ 3D grid and encoding (i) Van der Waals interactions (calculated as Lennard-Jones potential with hydrogen, carbon, and large-atom probes) (ii) electrostatic potential, (iii) hydrogen bonding potential, and (iv) polar surface energy. The linkers (residues 480–497, 532–546, and 588–600) and the side-chains of the WW3 and WW4 domains were then conformationally sampled in internal coordinates to optimize the position of these domains and linkers in the context of the HECT domain. At least 10^7 energy optimization steps were performed for both models. Finally, top-scoring conformations of the fragment were inspected manually, integrated with the HECT domain in a single full-atom polypeptide chain, and subjected to a round of unrestrained full-atom side-chain minimization to resolve minor steric conflicts resulting from the merge.

QUANTIFICATION AND STATISTICAL ANALYSIS

All experimental data was analyzed using Prism 7.0 statistical software. Details of statistical analysis can be found in the figure legends. The exact value of *n* is given in each figure legend, where n = the number of independent repeats unless otherwise stated. All values were calculated and presented as the mean ± SD. Statistical tests included Students t tests, and one-way and two-way analysis of variance (ANOVA) and are stated when used.

Supplementary Material

Refer to Web version on PubMed Central for supplementary material.

ACKNOWLEDGMENTS

We thank members of the Trejo laboratory and co-authors for comments and advice. This work was supported, in whole or in part, by NIH/NIGMS R35 GM127121 (J.T.), GM117424 and AI118985 (to T.M.H. and I.K.), GM111665 (to J.Z.), San Diego IRACDA NIH/NIGMS K12 GM06852 (J.L.), American Heart Association Postdoctoral Fellowship Award (N.J.G.), and Pharmacological Sciences Training Grant NIH/NIGMS T32 GM007752 (C.C.R.).

REFERENCES

Abagyan R, and Totrov M (1994). Biased probability Monte Carlo conformational searches and electrostatic calculations for peptides and proteins. J. Mol. Biol 235, 983–1002. [PubMed: 8289329]

Adam AP (2015). Regulation of endothelial adherens junctions by tyrosine phosphorylation. Mediators Inflamm. 2015, 272858. [PubMed: 26556953]

Bose R, Holbert MA, Pickin KA, and Cole PA (2006). Protein tyrosine kinase-substrate interactions. Curr. Opin. Struct. Biol 16, 668–675. [PubMed: 17085043]

Bruce MC, Kanelis V, Fouladkou F, Debonneville A, Staub O, and Rotin D (2008). Regulation of Nedd4–2 self-ubiquitination and stability by a PY motif located within its HECT-domain. Biochem. J 415, 155–163. [PubMed: 18498246]

Buetow L, and Huang DT (2016). Structural insights into the catalysis and regulation of E3 ubiquitin ligases. Nat. Rev. Mol. Cell Biol 17, 626–642. [PubMed: 27485899]

Chen B, Dores MR, Grimsey N, Canto I, Barker BL, and Trejo J (2011). Adaptor protein complex-2 (AP-2) and epsin-1 mediate protease-activated receptor-1 internalization via phosphorylation- and ubiquitination-dependent sorting signals. J. Biol. Chem 286, 40760–40770. [PubMed: 21965661]

Chen B, Siderovski DP, Neubig RR, Lawson MA, and Trejo J (2014). Regulation of protease-activated receptor 1 signaling by the adaptor protein complex 2 and R4 subfamily of regulator of G protein signaling proteins. J. Biol. Chem 289, 1580–1591. [PubMed: 24297163]

Chen Z, Jiang H, Xu W, Li X, Dempsey DR, Zhang X, Devreotes P, Wolberger C, Amzel LM, Gabelli SB, et al. (2017). A tunable brake for HECT ubiquitin ligases. Mol. Cell 66, 345–357. [PubMed: 28475870]

Dores MR, and Trejo J (2014). Atypical regulation of G protein-coupled receptor intracellular trafficking by ubiquitination. Curr. Opin. Cell Biol 27, 44–50. [PubMed: 24680429]

Escobedo A, Gomes T, Aragón E, Martín-Malpartida P, Ruiz L, and Macias MJ (2014). Structural basis of the activation and degradation mechanisms of the E3 ubiquitin ligase Nedd4L. Structure 22, 1446–1457. [PubMed: 25295397]

Gallagher E, Gao M, Liu YC, and Karin M (2006). Activation of the E3 ubiquitin ligase Itch through a phosphorylation-induced conformational change. Proc. Natl. Acad. Sci. USA 103, 1717–1722. [PubMed: 16446428]

Grimsey NJ, Aguilar B, Smith TH, Le P, Soohoo AL, Puthenveedu MA, Nizet V, and Trejo J (2015). Ubiquitin plays an atypical role in GPCR-induced p38 MAP kinase activation on endosomes. J. Cell Biol 210, 1117–1131. [PubMed: 26391660]

Grimsey NJ, Coronel LJ, Cordova IC, and Trejo J (2016). Recycling and endosomal sorting of protease-activated receptor-1 Is distinctly regulated by Rab11A and Rab11B proteins. J. Biol. Chem 291, 2223–2236. [PubMed: 26635365]

Jean-Charles PY, Snyder JC, and Shenoy SK (2016). Chapter one— ubiquitination and deubiquitination of G protein-coupled receptors. Prog. Mol. Biol. Transl. Sci 141, 1–55. [PubMed: 27378754]

Kamadurai HB, Souphron J, Scott DC, Duda DM, Miller DJ, Stringer D, Piper RC, and Schulman BA (2009). Insights into ubiquitin transfer cascades from a structure of a UbcH5B approximately ubiquitin-HECT(NEDD4L) complex. Mol. Cell 36, 1095–1102. [PubMed: 20064473]

Lapek JD, Jr., Lewinski MK, Wozniak JM, Guatelli J, and Gonzalez DJ (2017). Quantitative temporal viromics of an inducible HIV-1 model yields insight to global host targets and phospho-dynamics associated with protein Vpr. Mol. Cell. Proteomics 16, 1447–1461. [PubMed: 28606917]

Liu D-Z, Ander BP, Xu H, Shen Y, Kaur P, Deng W, and Sharp FR (2010). Blood-brain barrier breakdown and repair by Src after thrombininduced injury. Ann. Neurol 67, 526–533. [PubMed: 20437588]

Liu Y, Lau J, Li W, Tempel W, Li L, Dong A, Narula A, Qin S, and Min J (2016). Structural basis for the regulatory role of the PPxY motifs in the thioredoxin-interacting protein TXNIP. Biochem. J 473, 179–187. [PubMed: 26527736]

Lu S, Ouyang M, Seong J, Zhang J, Chien S, and Wang Y (2008). The spatiotemporal pattern of Src activation at lipid rafts revealed by diffusion-corrected FRET imaging. PLoS Comput. Biol 4, e1000127. [PubMed: 18711637]

Luttrell DK, and Luttrell LM (2004). Not so strange bedfellows: G-protein-coupled receptors and Src family kinases. Oncogene 23, 7969–7978. [PubMed: 15489914]

McCluskey A, Daniel JA, Hadzic G, Chau N, Clayton EL, Mariana A, Whiting A, Gorgani NN, Lloyd J, Quan A, et al. (2013). Building a better dynasore: The dyngo compounds potently inhibit dynamin and endocytosis. Traffic 14, 1272–1289. [PubMed: 24025110]

Mehta S, and Zhang J (2014). Using a genetically encoded FRET-based reporter to visualize calcineurin phosphatase activity in living cells. Methods Mol. Biol 1071, 139–149. [PubMed: 24052386]

Persaud A, Alberts P, Mari S, Tong J, Murchie R, Maspero E, Safi F, Moran MF, Polo S, and Rotin D (2014). Tyrosine phosphorylation of NEDD4 activates its ubiquitin ligase activity. Sci. Signal 7, ra95. [PubMed: 25292214]

Riling C, Kamadurai H, Kumar S, O'Leary CE, Wu KP, Manion EE, Ying M, Schulman BA, and Oliver PM (2015). Itch WW domains inhibit its E3 ubiquitin ligase activity by blocking E2-E3 ligase trans-thiolation. J. Biol. Chem 290, 23875–23887. [PubMed: 26245901]

Rotin D, and Kumar S (2009). Physiological functions of the HECT family of ubiquitin ligases. Nat. Rev. Mol. Cell Biol 10, 398–409. [PubMed: 19436320]

Sander B, Xu W, Eilers M, Popov N, and Lorenz S (2017). A conformational switch regulates the ubiquitin ligase HUWE1 eLife 6, Published online February 14, 2017. 10.7554/eLife.21036.

Scheffner M, and Kumar S (2014). Mammalian HECT ubiquitin-protein ligases: Biological and pathophysiological aspects. Biochim. Biophys. Acta 1843, 61–74. [PubMed: 23545411]

Smart JE, Oppermann H, Czernilofsky AP, Purchio AF, Erikson RL, and Bishop JM (1981). Characterization of sites for tyrosine phosphorylation in the transforming protein of Rous sarcoma virus (pp60v-src) and its normal cellular homologue (pp60c-src). Proc. Natl. Acad. Sci. USA 78, 6013–6017. [PubMed: 6273838]

Soto AG, and Trejo J (2010). N-linked glycosylation of protease-activated receptor-1 second extracellular loop: A critical determinant for ligand-induced receptor activation and internalization. J. Biol. Chem 285, 18781–18793. [PubMed: 20368337]

Soto AG, Smith TH, Chen B, Bhattacharya S, Cordova IC, Kenakin T, Vaidehi N, and Trejo J (2015). N-linked glycosylation of protease-activated receptor-1 at extracellular loop 2 regulates G-protein signaling bias. Proc. Natl. Acad. Sci. USA 112, E3600–E3608. [PubMed: 26100877]

Sriram K, and Insel PA (2018). GPCRs as targets for approved drugs: How many targets and how many drugs? Mol. Pharmacol 93, 251–258. [PubMed: 29298813]

Tobin AB (2008). G-protein-coupled receptor phosphorylation: Where, when and by whom. Br. J. Pharmacol 153 (Suppl 1), S167–S176. [PubMed: 18193069]

Traxler P, Bold G, Frei J, Lang M, Lydon N, Mett H, Buchdunger E, Meyer T, Mueller M, and Furet P (1997). Use of a pharmacophore model for the design of EGF-R tyrosine kinase inhibitors: 4-(phenylamino)pyrazolo [3,4-d]pyrimidines. J. Med. Chem 40, 3601–3616. [PubMed: 9357527]

Wang J, Peng Q, Lin Q, Childress C, Carey D, and Yang W (2010). Calcium activates Nedd4 E3 ubiquitin ligases by releasing the C2 domain-mediated auto-inhibition. J. Biol. Chem 285, 12279–12288. [PubMed: 20172859]

Wiesner S, Ogunjimi AA, Wang HR, Rotin D, Sicheri F, Wrana JL, and Forman-Kay JD (2007). Autoinhibition of the HECT-type ubiquitin ligase Smurf2 through its C2 domain. Cell 130, 651–662. [PubMed: 17719543]

Yang C, Zhou W, Jeon MS, Demydenko D, Harada Y, Zhou H, and Liu YC (2006). Negative regulation of the E3 ubiquitin ligase itch via Fyn-mediated tyrosine phosphorylation. Mol. Cell 21, 135–141. [PubMed: 16387660]

Zhu K, Shan Z, Chen X, Cai Y, Cui L, Yao W, Wang Z, Shi P, Tian C, Lou J, et al. (2017). Allosteric auto-inhibition and activation of the Nedd4 family E3 ligase Itch. EMBO Rep. 18, 1618–1630. [PubMed: 28747490]

Highlights

- GPCRs stimulate NEDD4–2 activity via rapid activation of c-Src at the plasma membrane
- c-Src phosphorylates NEDD4–2 tyrosine-485 within the auto-inhibitory linker peptide
- NEDD4–2 Y485 phosphorylation mediates GPCR-induced p38 inflammatory signaling

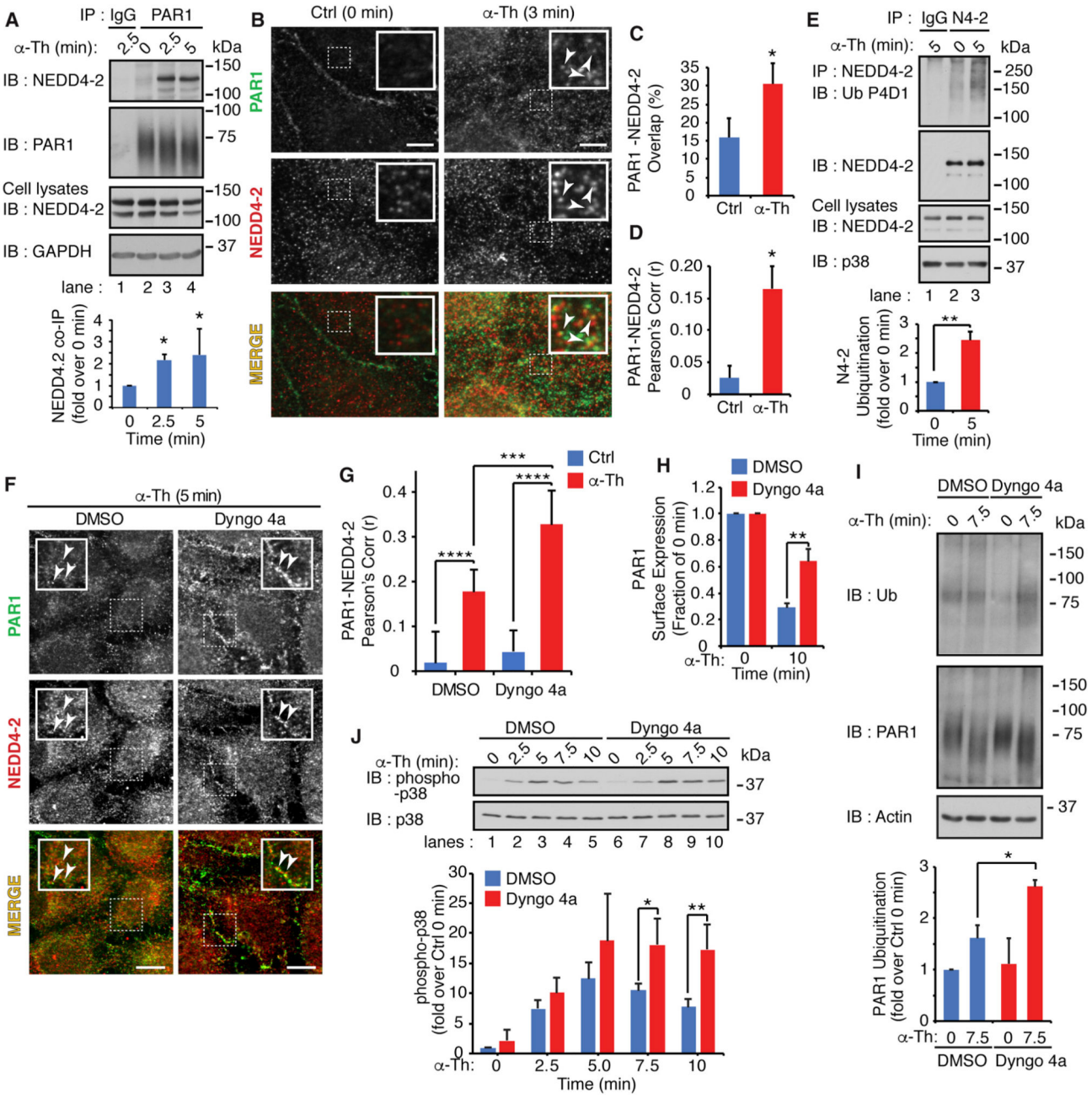

Figure 1. PAR1 Regulates NEDD4–2 Recruitment and Activation Independent of Internalization:

(A) Immunoblot of IP'ed PAR1 and co-associated NEDD4–2 from α-Thrombin (α-Th)-stimulated EA.hy926 cells. The data (mean ± SD, n = 3) were analyzed by ANOVA (*$p < 0.05$).

(B) Immunofluorescence confocal microscopy of PAR1 (green) and NEDD4–2 (red) in control (ctrl) or α-Th-stimulated human umbilical vein endothelial cells (HUVECs). PAR1 and NEDD4–2 colocalization is shown as yellow in the merged image. Insets are magnifications of boxed areas. Bars, 10 μm.

(C) Percentage of overlap of PAR1 (green pixels) and NEDD4–2 (red pixels), in control (ctrl) or α-Th-stimulated cells. The data (mean ± SD, n = 9) were analyzed by Student's t test (*p < 0.05).
(D) Pearson's correlation coefficients (*r*) calculated for PAR1 and NEDD4–2 colocalization in control (ctrl) or α-Th-stimulated cells. The data (mean ± SD, n = 9) were analyzed by Student's t test (*p < 0.05).
(E) Immunoblot of ubiquitinated NEDD4–2 IP'ed from α-Th-stimulated EA.hy926 cells. The data (mean ± SD, n = 3) were analyzed by Student's t test (**p < 0.01).
(F) Immunofluorescence confocal microscopy of PAR1 (green) and NEDD4–2 (red) in control (Ctrl) or α-Th-stimulated EA.hy926 cells pretreated with DMSO or Dyngo 4a. Colocalization of PAR1 and NEDD4–2 is shown as yellow in the merged image; insets are magnifications of boxed areas. Bars, 10 μm.
(G) Pearson's correlation coefficients (*r*) calculated for PAR1 and NEDD4–2 colocalization in α-Th-stimulated cells. The data (mean ± SD, n = 9) were analyzed by Student's t test (***p < 0.001, ****p < 0.0001).
(H) PAR1 surface expression in DMSO (Ctrl) or Dyngo 4a-treated cells. The data (mean ± SD n = 3) were analyzed by ANOVA (**p < 0.01)
(I) Immunoblot of ubiquitinated PAR1 IP'ed from DMSO or Dyngo 4a-treated EA.hy926 cells. The data (mean ± SD, n = 3) were analyzed by Student's t test (*p < 0.05).
(J) Immunoblots of cell lysates from DMSO (Ctrl) or Dyngo 4a-treated EA.hy926 cells. The data (mean ± SD n = 3) were analyzed by ANOVA (*p < 0.05, **p < 0.01).

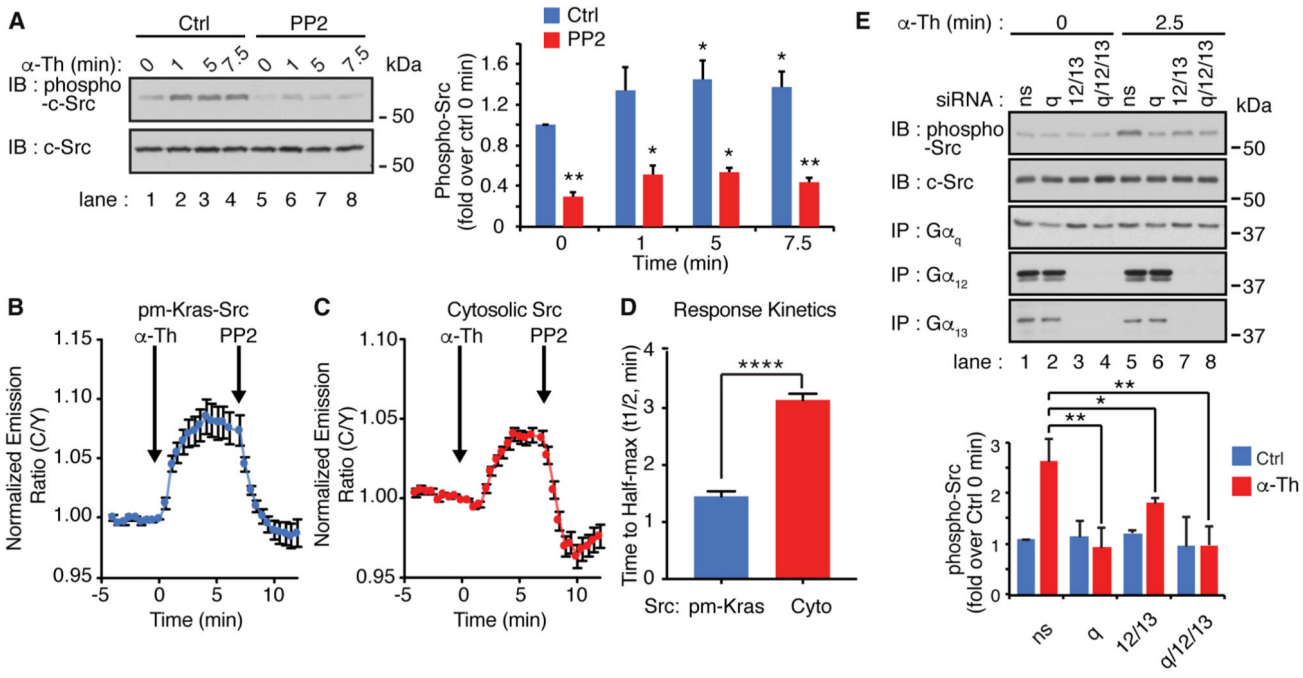

Figure 2. Rapid Activation of Plasma-Membrane-Associated c-Src by PAR1:

(A) Immunoblots of cell lysates from EA.hy926 cells in Ctrl or PP2-treated cells. The data (mean ± SD, n = 3) were analyzed by ANOVA (*p < 0.05, **p < 0.01).

(B and C) Activation of c-Src using a pm-Kras-Src (B) or cytosolic-Src FRET (C) biosensors expressed in EA.hy926 cells incubated with α-Th and PP2. FRET ratios were normalized prior to α-Th addition (mean ± SEM, n = >8 cells).

(D) Response kinetics of c-Src FRET biosensors in α-Th-stimulated EA.hy926 cells, time to half-max ($t_{1/2}$, min); the data (mean, ± SEM, n = 54 cells) were analyzed by Student's t test (****p < 0.0001).

(E) Immunoblots of cell lysates from non-specific (ns) $G\alpha_q$, $G\alpha_{12}$, or $G\alpha_{13}$ siRNA-transfected EA.hy926 cells. The data (mean ± SD, n = 3) were analyzed by Student's t test (*p < 0.05, **p < 0.01).

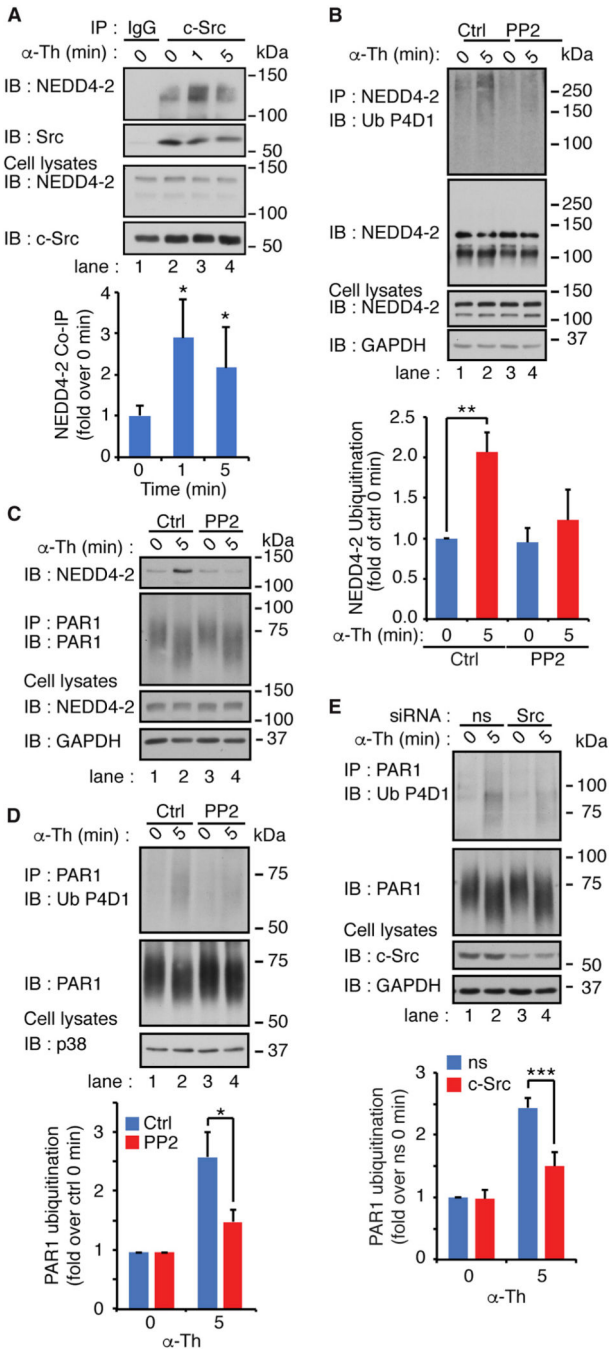

Figure 3. NEDD4–2 Auto-ubiquitination and PAR1 Ubiquitination Mediated by c-Src:

(A) Immunoblot of NEDD4–2 co-association with c-Src from α-Th-stimulated EA.hy926 cells. The data (mean ± SD, n = 3) were analyzed by Student's t test (*$p < 0.05$).

(B) Immunoblot of ubiquitinated NEDD4–2 from α-Th-stimulated EA.hy926 cells, Ctrl, or PP2 treatment. The data (mean ± SD, n = 3) were analyzed by Student's t test (**$p < 0.01$).

(C) Immunoblot of NEDD4–2 co-association with PAR1 from α-Th-stimulated EA.hy926 cells, Ctrl, or PP2 treatment.

(D) Immunoblot of ubiquitinated PAR1 from α-Th-stimulated EA.hy926 cells, Ctrl, or PP2 treated. The data (mean ± SD, n = 3) were analyzed by Student's t test (*$p < 0.05$).
(E) Immunoblot of ubiquitinated PAR1 from α-Th-stimulated EA.hy926 cells, transfected with control, ns-, or c-Src-specific siRNA. The data (mean ± SD, n = 3) were analyzed by Student's t test (***$p < 0.001$).

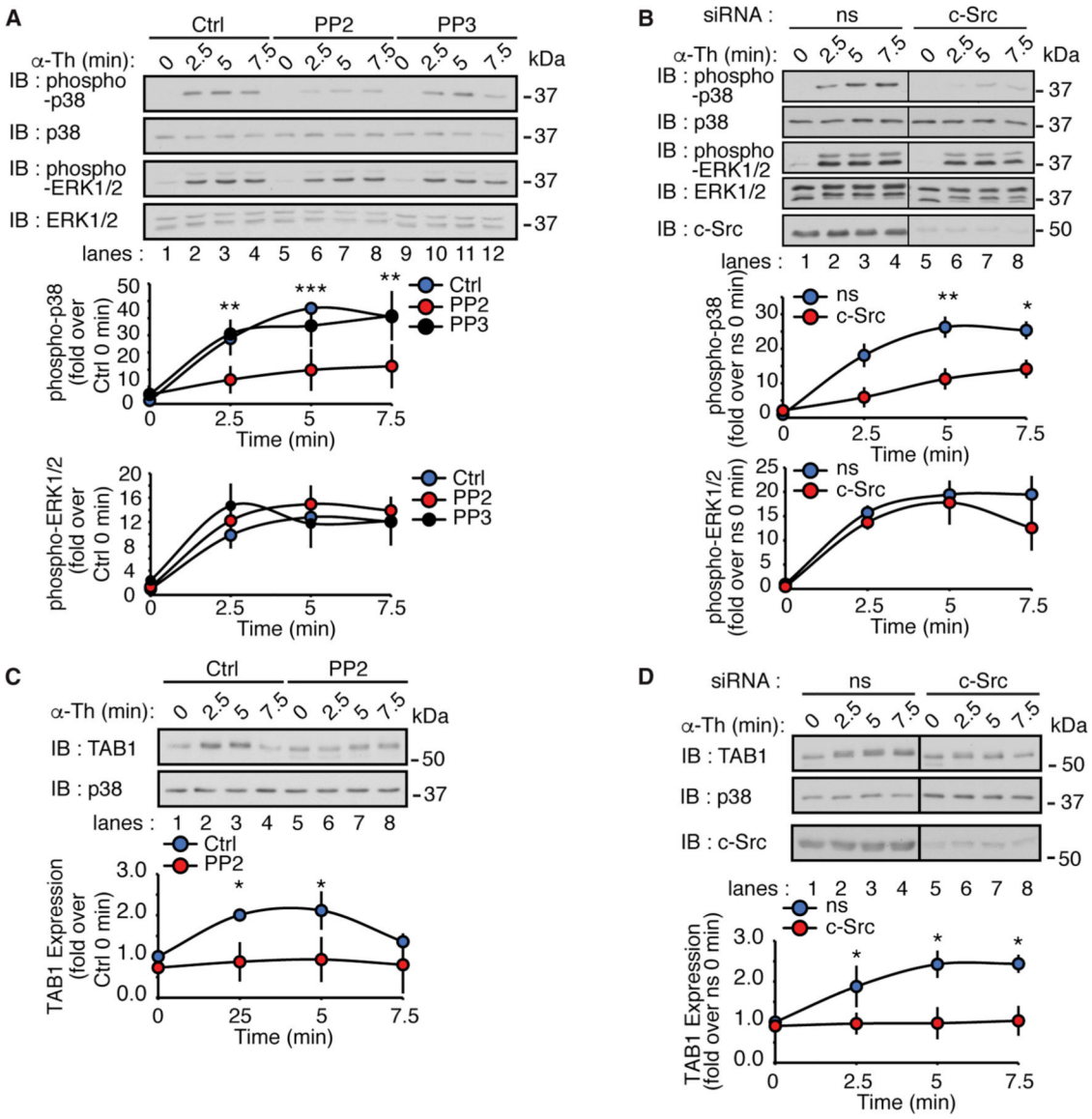

Figure 4. Thrombin Activation of p38 MAPK Requires c-Src:

(A and C) Immunoblot of cell lysates from EA.hy926 cells pretreated with Ctrl, PP2, or PP3 (A) or Ctrl and PP2 (C), prior to α-Th stimulation. The data (mean ± SD, n = 3) were analyzed by ANOVA (*p < 0.05, **p < 0.01, ***p < 0.001).

(B and D) Immunoblots of EA.hy926 cell lysates transfected with ns- or c-Src-specific siRNA prior to α-Th stimulation immunoblotted for p38 and ERK1/2 (B) or TAB1 (D). The data (mean ± SD, n = 3) were analyzed by ANOVA (*p < 0.05, **p < 0.01).

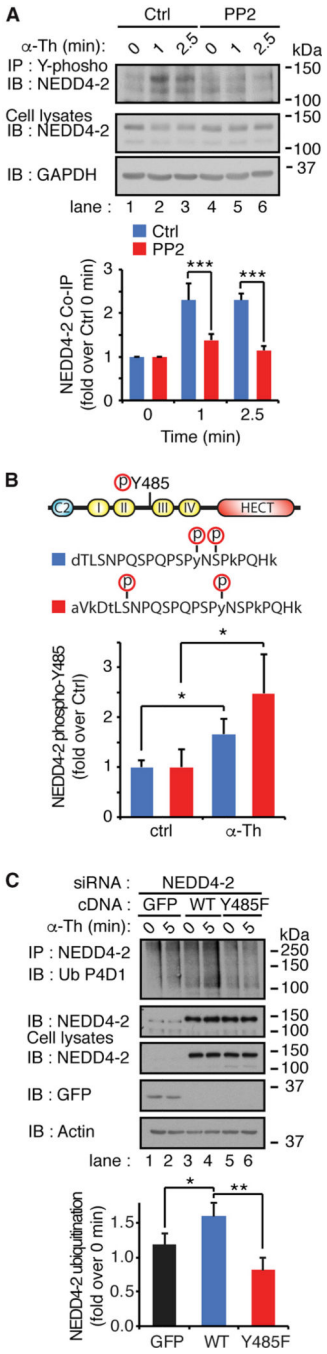

Figure 5. NEDD4–2 Tyrosine Phosphorylation Required for Auto-ubiquitination

(A) Immunoblot of tyrosine phosphorylated proteins from Ctrl or PP2-treatedEA.hy926 cells stimulated with α-Th. The data (mean ± SD, n = 3) were analyzed by ANOVA (***p < 0.001).

(B) Schematic representation of the NEDD4–2 domains and the two NEDD4–2 phosphopeptides identified by mass spectrometry, that showed α-Th-stimulated increase in Y485 phosphorylation. The data (mean ± SD, n = 3) were analyzed by Student's t test (*p < 0.05).

(C) Immunoblot of ubiquitinated NEDD4–2 from α-Th-stimulated EA.hy926 cells, stably expressing GFP, siRNA-resistant FLAG-NEDD4–2-wild-type (WT), or Y485F mutant. The data (mean ± SD, n = 3) were analyzed by Student's t test (*$p < 0.05$, **$p < 0.01$).

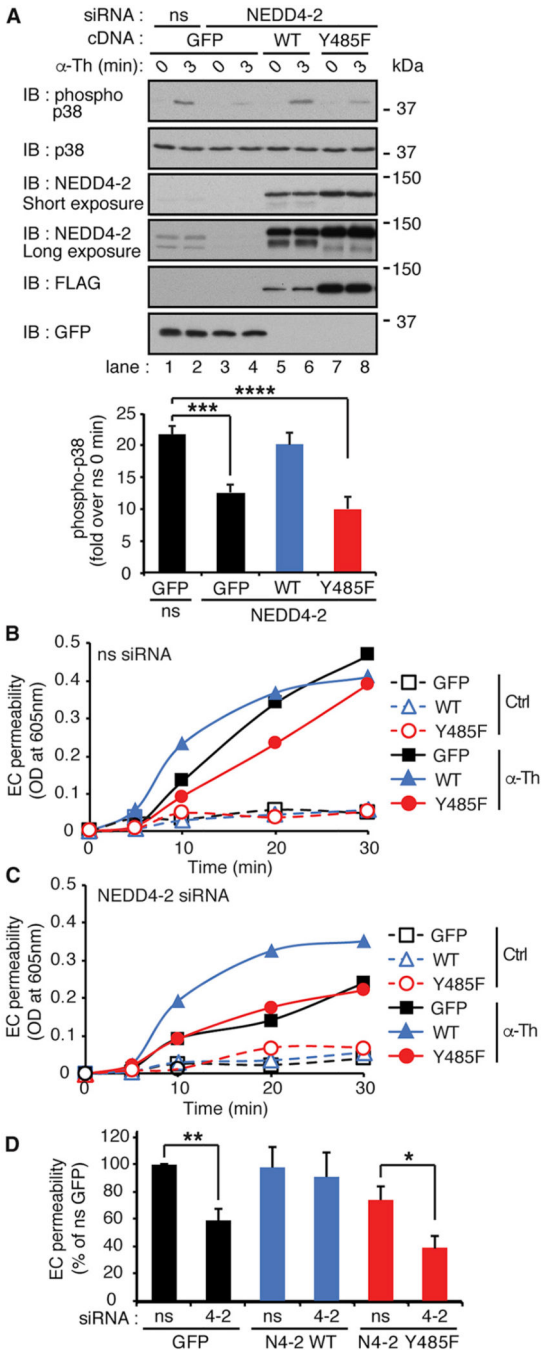

Figure 6. NEDD4–2 Y485 Is Critical for Thrombin-Induced Signaling and Endothelial Barrier Permeability

EA.hy926 cells expressing GFP or siRNA-resistant FLAG-NEDD4–2-wild-type or Y485F mutant, transfected with ns- or NEDD4–2 siRNA.

(A) Immunoblots of lysates from Ctrl or α-Th stimulated cells. The data (mean ± SD n = 3) were analyzed by ANOVA (***$p < 0.001$, ****$p < 0.0001$).

(B) Endothelial cell (EC) barrier permeability in ns siRNA-transfected Ctrl or α-Th stimulated cells.

(C) EC barrier permeability in NEDD4–2 siRNA-transfected Ctrl or α-Th stimulated cells.

(D) EC barrier permeability stimulated by α-Th in various cell lines relative to ns siRNA-transfected GFP cells at 20 min (mean ± SD, n = 3), analyzed by ANOVA (*p < 0.05, **p < 0.01).

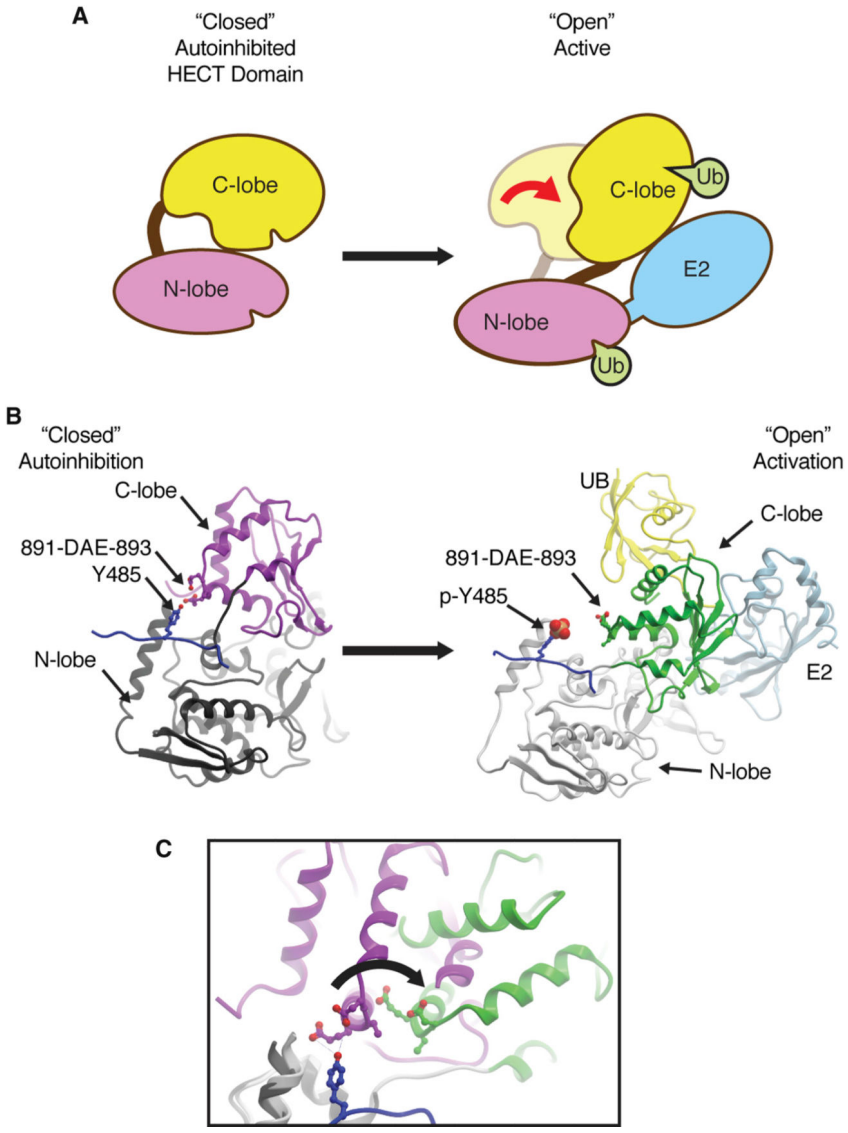

Figure 7. Structural Model of the 2,3-Linker Peptide NEDD4–2 Interaction with the C-lobe of the HECT Domain

(A) Cartoon model showing the functionally validated "closed" auto-inhibited and "open" activated conformation of HECT domain containing E3 ubiquitin ligases.

(B) A 3D structural model of the C-terminal region of the 2,3-linker peptide (dark blue) showing Y485 access to the acidic triad (D891, A892, E893) in C-lobe of the HECT domain (magenta) in the "closed" conformation of NEDD4–2, N-lobe (gray and black). In the active "open" conformation of NEDD4–2 C-lobe (green) when bound to ubiquitin (yellow) and the E2 ubiquitin ligase UbcH5B (light blue), phosphorylated Y485 is moved away. Surface view shows a structural model including the WW3 and WW4 domains in Figure S6.

(C) Predicted structural translation from the "closed"(magenta) to "open" (green) conformation of the C-lobe of NEDD4–2 HECT domain.